PAPER • OPEN ACCESS

Temperature-dependent change of the fractal dimension of Cu dendrites on Cu(111)

To cite this article: C Sprodowski and K Morgenstern 2020 *New J. Phys.* **22** 063055

New Journal of Physics
The open access journal at the forefront of physics

Deutsche Physikalische Gesellschaft DPG
IOP Institute of Physics

Published in partnership with: Deutsche Physikalische Gesellschaft and the Institute of Physics

OPEN ACCESS

RECEIVED
27 February 2020

REVISED
13 May 2020

ACCEPTED FOR PUBLICATION
19 May 2020

PUBLISHED
24 June 2020

PAPER

Temperature-dependent change of the fractal dimension of Cu dendrites on Cu(111)

C Sprodowski[1] and K Morgenstern[2]

[1] Institut für Festkörperphysik, Leibniz Universität Hannover, Appelstr. 2, D-30167 Hannover, Germany
[2] Ruhr-Universität Bochum, Lehrstuhl für physikalische Chemie I, Universitätsstr. 150, D-44801 Bochum, Germany

E-mail: karina.morgenstern@rub.de

Keywords: fractal dimension, time-lapsed STM, shape evolution

Abstract

We investigate the shape of monatomic high Cu islands on a Cu(111) surface by variable-temperature scanning tunneling microscopy between 110 K and 240 K. Low temperature dendrites evolve towards more compact shapes at increasing temperature; finally reaching the equilibrium shape of a hexagon with rounded corners. Time-lapsed imaging at increasing temperature reveals the onset of shape change to be at ≈170 K, corresponding to the onset of edge and corner diffusion of atoms along the island's borders. Despite a substantial variation for individual islands at each temperature, the mean fractal dimension increases monotonously between 170 K up to 240 K, from the smallest to the largest values feasible for islands grown on surfaces.

1. Introduction

General concepts based on a thorough atomistic-scale picture in model systems are important for designing growth routes for artificial material with custom-designed properties, e.g. nanoclusters or multilayers. Metastable low-dimensional structures are obtained through epitaxial growth at high supersaturation where kinetic limitations determine most structural features. For a general understanding of the processes and barriers leading to such structures, Cu/Cu(111) served as a benchmark system in homoepitaxy. Growth [1–3] and adatom island decay [4] were investigated thoroughly theoretically. Experiments investigated extensively for instance the size-dependent dynamical behaviour of islands from a few to a few ten atoms [5] and the Ehrlich–Schwoebel (ES) barrier and its effect on growth [6–9]. The ES barrier [10, 11] is an excess energy barrier that diffusing particles have to overcome, when diffusing over a step edge; reducing interlayer mass transport, if not surpassed in specific geometries [12, 13]. It causes the kinetically limited three-dimensional growth mode being predominate for Cu/Cu(111) between 115 K and 300 K as investigated by He scattering [14, 15] and by x-ray surface diffraction [9, 16]. The Cu/Cu(111) system also served as a model system to manipulate growth, such that the kinetic limitations of the ES barrier can be overcome [6, 14].

Studies for the Cu/Cu(111) concentrated so far on islands that were (mostly) in their equilibrium shape, which is a hexagon with rounded corners on fcc(111) surfaces. In contrast, ramified, far from equilibrium island structures were formed at high deposition rate or at low temperature on several other fcc(111) surfaces [17–19]. A barrier, similar to the ES barrier, for diffusion along the rim of islands leads to dendritic or fractal islands. Thereby, the islands are named dendritic, if they exhibit preferred growth directions induced by some surface symmetry related anisotropy in perimeter mobility [18]. They are named fractal, if they consist of randomly branched aggregates with no preferred direction of their branches.

Note that 'fractal' is a terminology adapted from mathematics for an object that cannot be described by an integer, but only by a Hausdorff–Besicovitch dimension [20]. It varies for a two-dimensional object between $D = 1$ (a line) and $D = 2$ (a filled circle) and is thus smaller than $D = 2$, the Euclidean dimension of a plane. D has been called fractal dimension. Due to growth constriction, the smallest possible value for metal islands grown on surfaces is $D = 5/3 = 1.67$ [21]. This value was determined in diffusion limited

aggregation (DLA), a computer simulation framework, in which particles undergo a random walk and stick to a growing aggregate at first encounter. Furthermore, the diffusivity along the island border is completely suppressed. In experiment, the diffusivity is suppressed, if the energy barrier for diffusion along the island border is so high that the probability of attachment of the next particle is considerably larger than the probability for a diffusive step along the island border.

In general, the fractal dimension is highly relevant in the description of the morphology of a multitude of highly irregular complex objects that are found in nature [22]. It has been used in diverse fields of science and technology for more than 30 years as geology [23], geophysics [24], hydrology [25], fluid mechanics [26], and carbon dioxide storage [27] in the context of non-equilibrium growth and aggregation, often with respect to the influence of surface roughness on fluid flow, sorption, and diffusion. For instance the interfacial contact stiffness [28] and the cloud nucleation activity of insoluble aerosols are directly related to the surface's fractal dimension [29]. More generally, ramified structures are also important in biology [30] and modern battery technology [31, 32].

In two dimensions, scanning tunneling microscopy (STM) facilitates the investigation of ramified islands in real space. For Au on graphite [33], Au on Ru(0001) [34], Pt on Pt(111) [17], Ag on Pt(111) [18, 35], and Ag on Ag(111) [36] fractal and for Pt on Pt(111) [17], Ag on Ag(111) [36, 37], Ag on Pt(111) [19], D_2O on Ag(111) [38, 39] and Ag(100) [40] dendritic islands were identified. In some of these cases, the importance of temperature on structure were demonstrated. Furthermore, kinetic Monte Carlo simulations enabled to determine onset temperatures of individual processes to predict island shapes at specific temperatures [2, 4, 41].

In this article, we grow dendritic Cu islands on Cu(111) on terraces and close to step edges at low temperature between 110 K and 170 K and characterize their shape by the fractal dimension. In time-lapsed image series at increasing temperature, we follow the change of this fractal dimension for individual islands over more than 10 K. We analyze this change for larger ensembles at specific temperatures and individual islands in dependence of temperature, demonstrating both, the large variety of coexisting fractal dimensions and the temperature dependence of its mean. The change in shape from the lowest to the largest possible value occurs in a rather small temperature window.

2. Experimental methods

STM measurements are performed with a fast scanning STM under ultra-high vacuum (UHV) conditions (2×10^{-10} mbar).

The Cu(111) sample is prepared by cycles of Ar^+-sputtering (1.3 keV, 3 to 5 $\times$ 10^{-5} mbar, 8 to 15 μA, 10 min to 30 min) and annealing up to 970 K (10 min to 45 min).

Cu is deposited by resistively heating a short Cu wire attached to a tungsten filament. The surface is held between 100 K and 170 K during deposition. The fluxes are monitored by a quartz balance. $\Delta\nu = 10$ Hz leads to a coverage of the order of 5% of a monolayer as calibrated on non fractal structures. The range of deposition for experiments in this article covers deposition of 5% to 20% ML at deposition rates between 2 ML/h to 10 ML/h. During metal deposition the chamber pressure stayed below 3×10^{-10} mbar. Note that there is a non-linear increase in temperature during deposition on a transfer rod without active cooling. We give the mean temperature of the deposition in the figure captions and stress that absolute temperatures might vary in another set-up, but the relative temperatures should hold. This uncertainty does not affect the main topic of the manuscript, because the temperature during the movies is determined precisely.

We image the sample at temperatures between 107 K and room temperature. This temperature is measured on an aluminum block that supports the STM and the sample and acts as a heat reservoir to stabilize the sample's temperature. A calibration with a thermo couple connected directly to a dummy non-crystalline sample of same material and size, revealed a negligible difference in temperature between the temperatures measured at the block and at the sample, presumably because of the high thermal conductivity of the block and a very tight fixation of the sample to it, which is necessary to avoid vibrational noise.

We follow the change in shape at increasing temperature in time-lapsed series, in which the same spot of the sample is imaged repeatedly. The temperature range of one movie is limited to around 15 K, because of the thermal drift during the temperature change in connection with a limited z range of the piezo element that adjusts the tip height above the sample. The whole temperature range from 160 K to 240 K is thus covered in several movies covering separate temperature ranges.

The box counting method is used to determine the fractal dimension of the islands [20, 42, 43]. The same methods was used before for water islands on silver surfaces [38–40] based on earlier work [18]. In this method, a grid of varying grid size ϵ is superimposed over the object of interest and the number

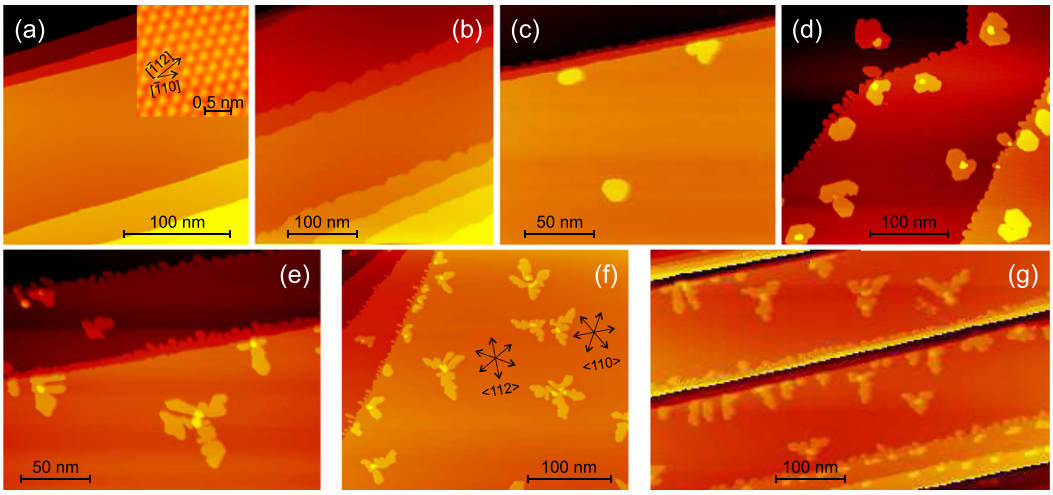

Figure 1. Growth of Cu islands on Cu(111): (a) surface before deposition, 0.36 nA, 994 mV; inset: atomic resolution; with one Gaussian smooth and surface direction as for all images of this article (b) after deposition at 300 K, 10% ML/44 s, 0.32 nA, −884 mV (c) after deposition at 137 K, 5% ML/66 s, 0.35 nA, 884 mV, 119 K (d) after deposition at 130 K, 20% ML/60 s, 0.5 nA, 884 mV (e) after deposition at 119 K, 20% ML/85 s, 0.49 nA, 884 mV (f) after deposition at 116 K, 20% ML/75 s, 0.61 nA, 884 mV with surface directions derived from images of atomic resolution (g) after deposition at 111 K, 10% ML/36 s, 0.28 nA, 884 mV, cyclic contrast to make structures on several terraces visible.

$N(\epsilon)$ of boxes filled or touched by this object is counted. The fractal dimension D is calculated via

$$D = \lim_{\epsilon \to 0} \frac{\log\ N(\epsilon)}{\log\ 1/\epsilon} \tag{1}$$

A graph of $\log(N(\epsilon))$ with respect to $\log\ 1/\epsilon$ yields a straight line with slope D. The whole procedure is automated in a Labview program. Note that the absolute value of the fractal dimension depends somewhat on the resolution of the STM images due to their pixel nature. This increases the spread in the data points shown.

3. Results and discussion

After the cleaning procedure, the sample consists of broad terraces, separated by step bundles with straight step edges (figure 1(a)). Deposition rates around 0.2 ML/min lead to distinctively different growth structures in dependence of temperature. For room temperature growth, all material reaches the step edges at terrace widths of $\approx$ 50 nm, leading to a roughening of the originally straight step edge (figure 1(b)). Thus, adatom diffusion along the step edge is not fast enough at the chosen deposition rate for finding optimal binding sites even at room temperature.

Islands nucleate on the terraces and at the upper part of preexisting step edges at deposition temperatures below 140 K (figures 1(c)–(g)). While the islands are rather compact around this temperature (figure 1(c)) they are more ramified for increasingly lower temperatures (figures 1(d)–(g)). Their ramified shape is likewise a result of kinetic limitations [21], where atom diffusion along the island edge is slow compared to the arrival time of additional atoms.

Even at low coverages below 20% ML, the majority of the islands has a second layer nucleus, mostly in the middle of the island. Thus, the ES barrier, so far by STM investigated for compact islands on Cu(111) [7, 8], also persists for non-straight island edges. The direction of the branches of these islands are not random, but follow mainly the Cu⟨112⟩ surface directions (figure 1(f)). As discussed in the introduction, such ramified islands are called dendrites. Also the compact second layer nuclei grow into dendrites at larger coverage (not shown).

In this article, we explore the transition of as grown dendrites, e.g. figure 2(a), towards equilibrium shaped islands; a hexagon with rounded corners, e.g. figure 2(b). To quantify the island shape, we determine its fractal dimension by the box counting method described in the experimental methods section, refer to equation (1). It is determined from the linear slope in the double-log plot of to number of filled squares N_{filled} with a side length of ϵ (figures 2(c) and (d)). Note that the change in numerical values from $D = 1.83$ for the island grown at 130 K (figure 2(c)) to $D = 1.86$ for the one annealed to 280 K (figure 2(d)) reflects a substantial change in shape. Thereby, troughs as in the lower part of the island

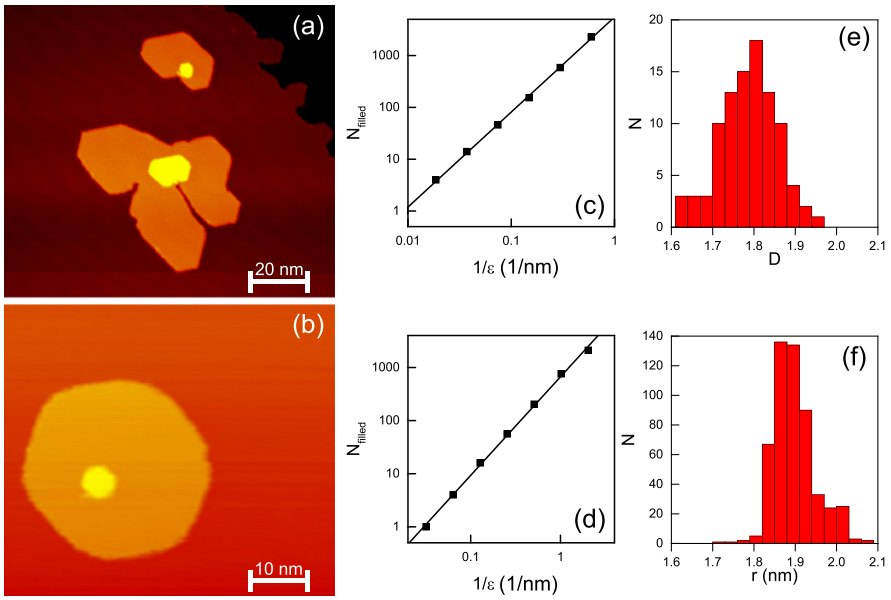

Figure 2. Shape and fractal dimension of Cu islands on Cu(111) terraces: (a) after deposition at 130 K; 20% ML in 60 s; 0.43 nA, 884 mV (b) after deposition at 125 K and annealing to 280 K, 0.38 nA, 760 mV (c, d) double-log plots for determination of fractal dimension of islands in panels (a, b) yielding (c) $D = (1.83 \pm 0.02)$ and (d) $D = (1.86 \pm 0.03)$; N_{filled}: number of filled boxes of side length ϵ, following equation (1) (e, f) histogram of fractal dimension D at (e) 84 to 110 K (f) 230 K to 245 K.

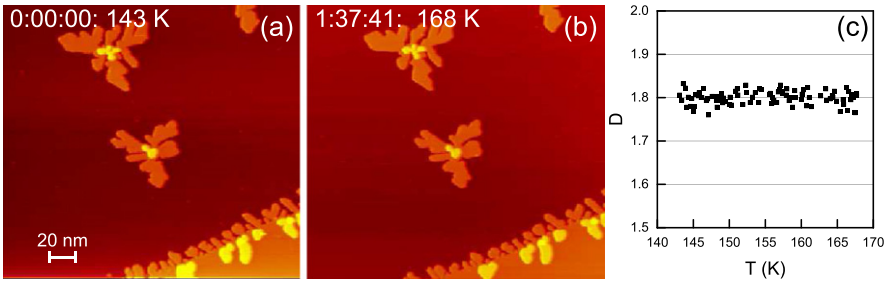

Figure 3. First and last image of a movie recorded between (a) 143 and (b) 168 K after Cu deposition of 20% ML at 116 K within 66 s; 0.55 …0.64 nA, 884 mV, 141 images. (c) Fractal dimension D versus temperature T for island with $A = (992 \pm 29)$ nm^2; average $D_{\text{av}} = 1.80 \pm 0.02$.

in figure 2(a) do not contribute to the fractal dimension as boxes in this region are partly filled for all box sizes considered in the analysis.

As each island has its individual shape, there is a rather broad distribution of fractal dimensions for islands grown (and imaged) under similar conditions (figures 2(e) and(f)). These values spread from 1.65 to 1.95 for islands grown at 84 K to 110 K. The spread is less for islands observed between 230 K and 245 K, for which the fractal dimension varies from 1.85 to 2.05. Despite the spread, the two distributions clearly differ as also reflected in their mean of 1.78 and 1.90, respectively.

In order to track this change in shape we follow individual islands in time-lapsed series, called movies, recorded at increasing temperature. There is no apparent change in shape for an island recorded between 143 and 168 K on the timescale of the measurement (figures 3(a) and (b)), reflected in a constant fractal dimension of (1.8 ± 0.02) (figure 3(c)). The variation around the mean also reflects the precision of the fractal dimension determination of our study. As no changes occur, the edge diffusion of atoms along the island border is not activated.

In the temperature-increasing movies, we determine the onset of edge diffusion by the onset of changes in fractal dimension. The onset of edge diffusion at around 170 K is demonstrated by a movie that crosses this threshold temperature, covering the temperature range from 160 K to 175 K (figures 4(a)–(c)). There are very subtle changes only around this onset temperature (figures 4(a) and (c), arrows). Troughs in the circumference and protruding branches are smoothed (e.g. lower right arrows). The islands nucleated in the second layer show the same trend (other arrows). These subtle changes are visualized by superimposing the last image, inverted in color, semi-transparently to the first image. Purple and yellow for

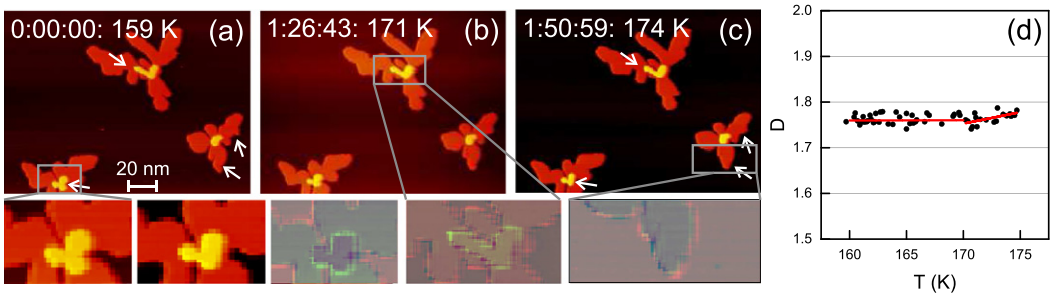

Figure 4. Four images of a movie recorded at (a) 160 K (b) 170 K and (c) 175 K after deposition of 20% ML in 75 s at 116 K; arrows point to some of the changes, marked squares are shown at threefold size and the last image superimposed semi-transparently in inverted color to the first image to make the subtle changes visible; in this superposition regions that changed are yellow to green, while unchanged regions should be invisible, but are in reality hazy; 0.48 …0.68 nA, 884 mV, 116 images. (d) Fractal dimension D versus temperature T for island with $A = (841 \pm 33)\text{nm}^2$; average $D_{av} = 1.76 \pm 0.01$; lines are fit to data in the respective region.

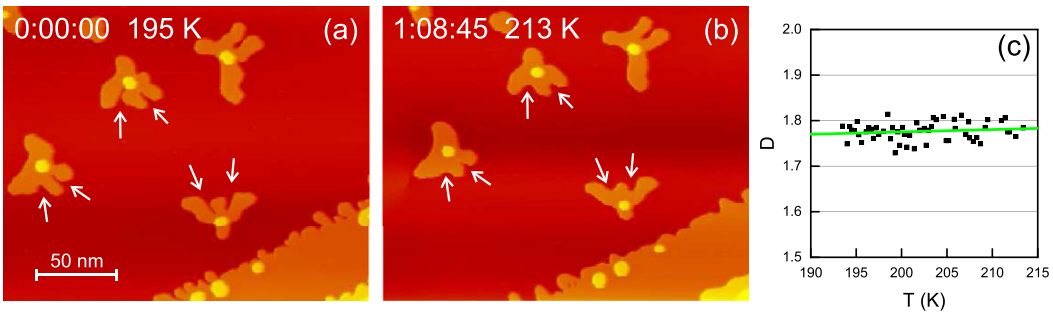

Figure 5. First (a) and last (b) image of a movie recorded at 195 to 213 K after deposition of 20% ML in 66 s at 116 K; arrows point to some of the changes, 0.42 …0.54 nA, 883 mV, 74 images. (c) Fractal dimension D versus temperature T for island with $A = (737 \pm 50)\text{nm}^2$; linear fit with slope of $(5.16 \pm 4.95) \times 10^{-4}$ K^{-1}.

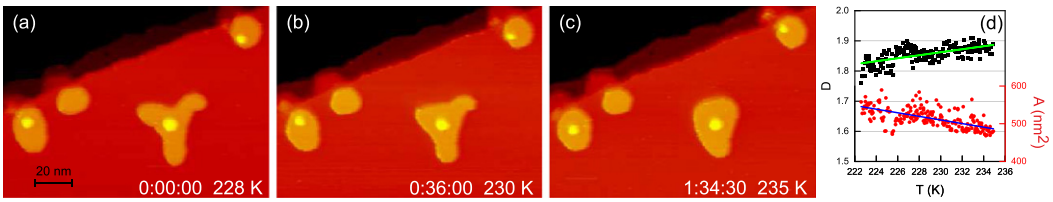

Figure 6. (a–c) Snapshots of a movie recorded at 227 K to 235 K after deposition of 20 ML at 118 K; 0.51 …0.63 nA, 760 mV, 278 images. (d) Fractal dimension D and area A versus temperature T for island with $A = (515 \pm 30)\text{nm}^2$; linear fit with slope of $(4.96 \pm 0.41) \times 10^{-3}$ K^{-1}.

the upper islands and orange for the lower islands represent those regions that are altered. The mean of the changes in the fractal dimension is within the error margin, but linear fits to different parts of the experimental values reveal the change fractal dimension above 170 K (figure 4(d)).

The higher the temperature, the more prominent are the changes (figure 5). In the movie recorded at around 200 K much deeper troughs are filled (figures 5(a) and (b), arrows). The change in fractal dimension, at around 5×10^{-4} K^{-1}, is still small (figure 5(c)).

This change is, at 5×10^{-3} K^{-1}, an order of magnitude larger for an island changing its shape at around 200 K (figure 6(d)). The largest island on figure 6(a) still exhibit three arms, though much thicker and more compact than in the examples at lower temperature. These arms retract toward the island core upon further temperature increase, thereby increasing the compactness further (figures 6(b) and (c)).

While for filling of the troughs the adatoms have to diffuse around concave steps, the retraction demand also either their diffusion around convex steps or detachment from them. The latter process is consistent with a slight decrease in area during the shape equilibration (figure 6(d)), despite the onset of temperature for Ostwald ripening being considerably higher [44]. Thus, this energy barrier can be overcome above ≈ 225 K.

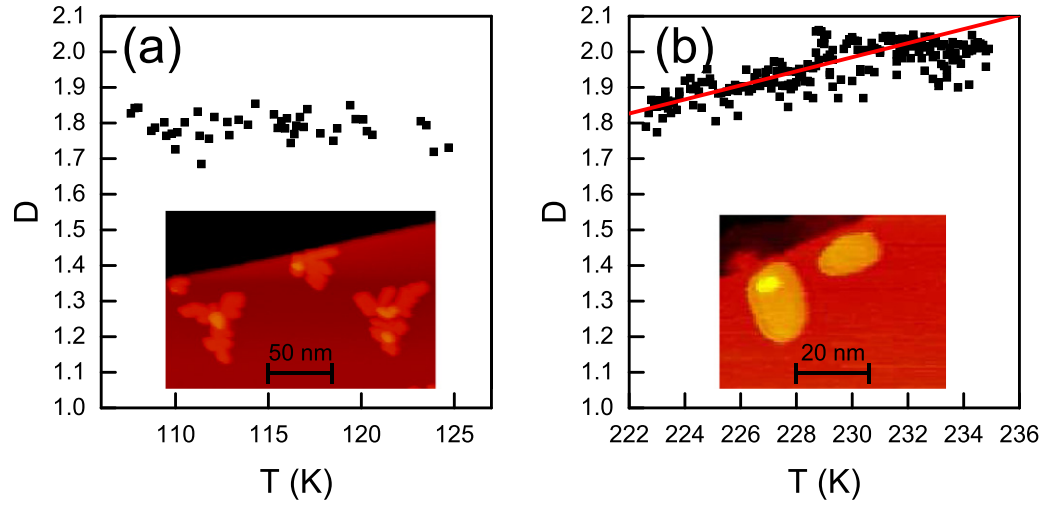

Figure 7. (a, b) Fractal dimension for islands nucleated at step edges at (a) low temperature, $A = (769 \pm 86)\mathrm{nm}^2$; 0.33 nA, −884 mV (b) high temperature, $A = (164 \pm 10)\mathrm{nm}^2$, line is fit to values below 230 K; 0.58 nA, 760 mV; insets represent first image of the movies.

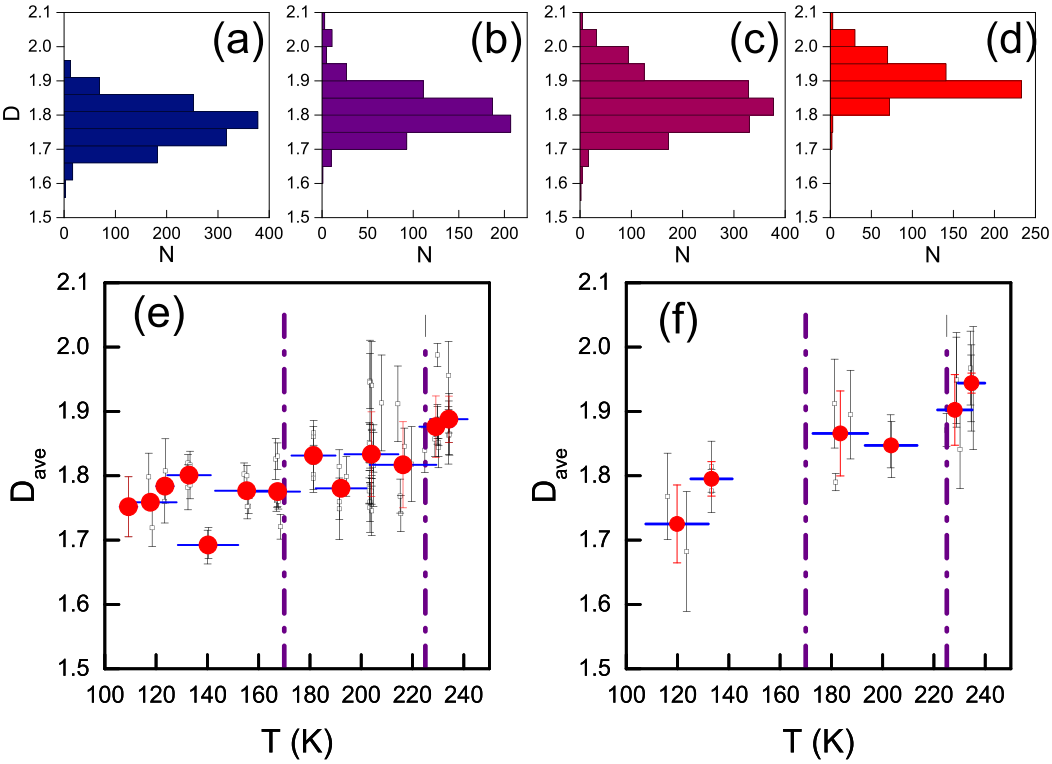

Figure 8. Temperature dependence of fractal dimension D: (a–d) histograms of fractal dimension D for islands (a) below 170 K (b) between 170 K and 200 K (c) between 200 K and 230 K (d) above 230 K (e, f) average value for individual movies (open squares) and average between several movies (filled circles) across temperatures ranges as marked by horizontal line; dashed-dotted lines marks onset temperatures of 170 K and 225 K: (e) on terrace (f) close to step edge.

So far, we discussed islands nucleated homogeneously on the middle of terraces. During low temperature growth, islands nucleate also at the upper step edge (figures 1(c)–(g)). These islands are less symmetric, showing only one to two branches due to geometric constraints. Nonetheless, these islands follow the same trend, which is no change in fractal dimension at low temperature (figure 7(a)) and an increase at higher temperature (figure 7(b)). For the latter island, the fractal dimension increases up to 230 K with a slope of $(1.98 \pm 0.17) \times 10^{-2}\ \mathrm{K}^{-1}$. Above 230 K, a constant value of 1.998 ± 0.039 is maintained, very close to the Eucledian, i.e. space filling, value.

Having demonstrated the change in fractal dimension for a few individual islands, we now determine island shapes for a multitude of islands to generalize the results. Despite the spread in fractal dimension in

each temperature range, there is a clear trend to larger values with increasing temperature from 1.77 ± 0.06 for islands below 170 K (figure 8(a)) over 1.81 ± 0.06 for islands between 170 K and 200 K (figure 8(b)) and 1.83 ± 0.08 for islands between 200 K (figure 8(c)) and 230 K to 1.90 ± 0.05 for islands above 230 K (figure 8(d)).

Because of the large variation in the initially grown islands there is quite a spread in average fractal dimension, for both symmetric islands on the terraces (figure 8(e)) and less symmetric ones close to step edges (figure 8(f)). However, averaging these mean values over several movies that were recorded at similar temperature ranges confirms the onset of equilibration to be around 170 K. Below this value, all D_{ave} are below 1.8. Above this value, they gradually increase. The second threshold temperature of 225 K manifests itself in the last two D_{ave} values, which are in both cases larger than D_{ave} below 225 K. Note that the values for islands at step edges are larger than those for terrace islands above 170 K. We attribute this to the larger sizes of the latter, which demand more mass transport and thus longer times to reach a similar change in fractal dimension than for smaller sizes.

4. Conclusion

We followed the equilibration of dendritic Cu islands on Cu(111) in time-lapsed series from islands with a fractal dimension of 1.7 up to 2.0. The kinetically limited structures start evolving towards their equilibrium shape at 170 K indicating the activation of edge diffusion at and above this temperature. The compact shape can be reached at temperatures as low as 230 K, below the onset of Ostwalds ripening, i.e. the detachment of Cu atoms from step edges.

Apart from the beauty of such non-equilibrium structures, these forms are expected to have important consequences for surface processes. For instance, they will alter the efficiencies of catalysts, not only because of the longer step edges, which are known to be much more effective than terraces for a multitude of chemical reactions, but possibly also due to geometric constraints, within the pockets. We propose to use the rates determined here and in future experiments to tailor surface for improved catalytic behavior.

The experimental approach used here to determine the onset of equilibration rates for shape changes of dendritic islands by following it in dependence of temperature complements theoretical Monte Carlo simulations. Though the latter give more precise values, our study demonstrates how, besides an expected much larger variety in growth structures, similar values can be extracted experimentally.

Acknowledgments

This work was supported by the Research Training Group 'Confinement-controlled Chemistry', which is funded by the Deutsche Forschungsgemeinschaft (DFG)-GRK2376/331085229.

References

[1] Stoltze P and Nørskov J K 1993 *Phys. Rev.* B **48** 5607–11
[2] Pomeroy J M, Jacobsen J, Hill C C, Cooper B H and Sethna J P 2002 *Phys. Rev.* B **66** 235412
[3] Lysenko O V, Stepanyuk V S, Hergert W and Kirschner J 2002 *Phys. Rev. Lett.* **89** 126102
[4] Larsson M I 2001 *Phys. Rev.* B **64** 115428
[5] Vamvakopoulos E and Evangelakis G A 2001 *J. Phys.: Condens. Matter* **13** 10757–66
[6] Wulfhekel W, Lipkin N N, Kliewer J, Rosenfeld G, Jorritsma L C, Poelsema B and Comsa G 1996 *Surf. Sci.* **348** 227–42
[7] Giesen M, Schulze Icking-Konert G and Ibach H 1998 *Phys. Rev. Lett.* **80** 552–5
[8] Giesen M, Schulze Icking-Konert G and Ibach H 1999 *Phys. Rev. Lett.* **82** 3101–4
[9] Camarero J, de la Figuera J, de Miguel J J, Miranda R, Alvarez J and Ferrer S 2000 *Surf. Sci.* **459** 191–205
[10] Ehrlich G and Hudda F G 1966 *J. Chem. Phys.* **44** 1039
[11] Schwoebel R L and Shipsey E J J 1966 *Appl. Phys.* **37** 3682
[12] Morgenstern K, Rosenfeld G, Comsa G, Lægsgaard E and Besenbacher F 2000 *Phys. Rev. Lett.* **85** 468
[13] Morgenstern K, Rosenfeld G, Comsa G, Sørensen M R, Hammer B, Lægsgaard E and Besenbacher F 2001 *Phys. Rev.* B **63** 045412
[14] Rosenfeld G, Lipkin N N, Wulfhekel W, Kliewer J, Morgenstern K, Poelsema B and Comsa G 1995 *Appl. Phys.* A **61** 455–66
[15] Miguel J J, Camarero J and Miranda R 2002 *J. Phys.: Condens. Matter* **14** 6155–72
[16] van der Vegt H A, Alvarez J, Torrelles X, Ferrer S and Vlieg E 1995 *Phys. Rev.* B **52** 17443–8
[17] Michely T, Hohage M, Bott M and Comsa G 1993 *Phys. Rev. Lett.* **70** 3943–7
[18] Brune H, Romainczyk C, Roeder H and Kern K 1994 *Nature* **369** 469–71
[19] Brune H 1998 *Surf. Sci. Rep.* **31** 121–229
[20] Mandelbrot B B 1983 *The Fractal Geometry of Nature* (Spektrum Akademischer Verlag Weinheim)
[21] Witten T A and Sander L M 1981 *Phys. Rev. Lett.* **47** 1400–3
[22] Addison P S 1997 *Fractals and Chaos—An Illustrated Course* (Bristol: : IOP Publishing)
[23] Toole J, Thomson J, Wilson T R S and Baxter M S 1984 *Nature* **308** 263
[24] Brown S R 1987 *J. Geophys. Res.* **92** 1337–47

[25] Zimmerman R W, Chen D W and Cook N G W 1992 *J. Hydrol.* **130** 79–96
[26] Zhang C, Chen Y, Deng Z and Shi M 2012 *Phys. Rev.* E **86** 016319
[27] Aminu M D, Nabavi S A, Rochelle C A and Manovic V 2017 *Appl. Energy* **208** 1389–419
[28] Zhang D, Xia Y, Scarpa F, Hong J and Ma Y 2017 *Sci. Rep.* **7** 12974
[29] Laaksonen A, Malila J, Nenes A, Hung H-M and Chen J-P 2016 *Sci. Rep.* **6** 25504
[30] West G B, Brown J H and Enquist B J 1999 *Science* **284** 1677
[31] Zachman M J, Tu Z, Choudhury S, Archer L A and Kourkoutis L F 2018 *Nature* **560** 345
[32] Xiao J 2019 *Science* **366** 426
[33] Wynblatt P, Metois J J and Heyraud J C 1990 *J. Cryst. Growth* **102** 618
[34] Hwang R Q, Schröder J, Günther C and Behm R J 1991 *Phys. Rev. Lett.* **67** 3279–82
[35] Röder H, Hahn E, Brune H, Bucher J-P and Kern K 1993 *Nature* **366** 141–3
[36] Röder H, Bromann K, Brune H and Kern K 1995 *Phys. Rev. Lett.* **74** 3217–20
[37] Cox E, Li M, Chung P-W, Ghosh C, Rahman T S, Jenks C J, Evans J W and Thiel P A 2005 *Phys. Rev.* B **71** 115414
[38] Heidorn S-C, Bertram C and Morgenstern K 2016 *Chem. Phys. Lett.* **665** 1–5
[39] Heidorn S-C, Lucht K, Bertram C and Morgenstern K 2018 *J. Phys. Chem.* B **122** 479–84
[40] Bakradze G and Morgenstern K 2018 *ChemPhysChem* **19** 2858–62
[41] Candia A E, Gomez L, Vidal R A, Ferron J and Passeggi M C G 2015 *J. Phys. D: Appl. Phys.* **48** 265305
[42] Takayasu H 1990 *Fractals in the Physical Sciences* (New York: Manchester University Press)
[43] Nayak S R, Mishra J and Palai G 2019 *Image Vis. Comput.* **89** 21–34
[44] Schlößer D C, Morgenstern K, Verheij L K, Rosenfeld G, Besenbacher F and Comsa G 2000 *Surf. Sci.* **465** 19–39